Journal of Alloys and Compounds 587 (2014) 380–386

Contents lists available at ScienceDirect

Journal of Alloys and Compounds

journal homepage: www.elsevier.com/locate/jalcom

Elastic, thermochemical and thermophysical properties of rock salt-type transition metal carbides and nitrides: A first principles study

G. Sai Gautam, K.C. Hari Kumar *

Department of Metallurgical and Materials Engineering, Indian Institute of Technology Madras, Chennai 600 036, India

ARTICLE INFO

Article history:
Received 30 August 2013
Received in revised form 17 October 2013
Accepted 18 October 2013
Available online 30 October 2013

Keywords:
Transition metal
Carbides
Nitrides
First principles

ABSTRACT

The rock salt-type transition metal carbides and nitrides are excellent refractory materials as well as important microstructural constituents in High Strength Low Alloy (HSLA) steels. Therefore, it is important to have knowledge on their elastic, thermophysical and thermochemical properties in order to gain deeper understanding of their role in these contexts. In this paper we report their mechanical properties such as the elastic constants, various moduli, Poisson's ratio and cleavage energies, thermochemical properties such as the energy of formation and cohesive energy and physical properties such as the p–V relation, first derivative of bulk modulus with respect to pressure, Debye temperature and the heat capacity determined using first principles calculations. Wherever possible, corresponding experimental data have been compared with and a good agreement is seen.

1. Introduction

Carbides and nitrides of transition elements have always been of interest in materials engineering for their high hardness, wear and friction properties, high melting points and good thermal conductivity [1–3]. They have found applications in refractories and abrasives. Being refractory binaries, they crystallize like ionic compounds in the rock salt structure. Specifically the carbides and nitrides of elements such as Ti, Nb, Mo, and V, are of particular interest to the steel industry since they form microstructural constituents for the High Strength Low Alloy (HSLA) steels. The above listed elements, along with elements like Ta, Zr and Hf have a proclivity for forming carbides and nitrides and hence can be used to form precipitates, by suitable thermomechanical treatments, to impart strength to the HSLA steels.

Precipitation strengthening often depends on the size and the distribution of the precipitate particles as well as how hard the precipitate actually is. Hence, it is imperative to study the mechanical properties of these carbides and nitrides in order to have a better understanding of the strengthening that can be caused by each of them. Generating experimental data of parameters such as Young's modulus and elastic constants for these systems have often been found difficult due to their extreme hardness. However, the density functional theory (DFT) provides a very useful procedure to study the mechanical properties of such systems. Various properties calculated by DFT can be used as input parameters in higher length-scale and longer time-scale simulations.

Measurement of the elastic properties of the carbides and nitrides under consideration is often done through diamond-anvil cells, measuring the velocities of the surface acoustic waves, X-ray diffraction measurements of residual stresses, ultrasonic methods, etc. The National Institute of Standards and Technology (NIST), USA [4] has put together a compilation of the experimental measurements done so far for these materials. It can be easily seen that the reported values are rather scattered. Hence, it is imperative to carry out first principle calculations in order to bring more clarity to an otherwise scattered experimental data. There have been several attempts at first principle calculations of select compounds such as CrC [6], CrN [9], HfC [6,10], MoC [6], NbC [6,10], NbN [8,11], TaC [5], TaN [8,11], TiC [6,7,10,12], TiN [7,10–12], VC [6], VN [8,9,11] and ZrC [10,13,14]. All of the above listed calculations, except for [9,8,12], have performed computations using ultra-soft potentials by employing either the Vienna *Ab-Initio* Simulations Package (VASP) [15] or the CASTEP module [16] of the Materials Studio package [17]. However, harder potentials such as the PAW [18] have been shown to produce better results compared to the ultra-soft potentials, since they use smaller core radii and an extended basis set. Perdew et al. [19] have recently demonstrated an optimization of the GGA specifically for ionic solids (GGA–PBEsol) to be used as an exchange–correlation potential. It is reported [35] that the PBEsol functional gives more accurate results than the PBE for calculating equilibrium properties like bond lengths, while it is not so good for parameters like cohesive energy. Another study [36] indicates that PBEsol gives better results than PBE (which in turn is better than LDA) when it comes to vibrational and dielectric properties. Hence, the current study aims to generate more accurate and more consistent results, encompassing all the

* Corresponding author. Tel.: +91 44 2257 4766.
E-mail address: kchkumar@iitm.ac.in (K.C. Hari Kumar).

0925-8388/$ - see front matter © 2013 Elsevier B.V. All rights reserved.
http://dx.doi.org/10.1016/j.jallcom.2013.10.156

systems that have been studied sporadically before, by employing the PAW potential coupled with the GGA–PBEsol functional. In some specific cases like the determination of the VASP energy of a nitrogen dimer, the GGA–PBE is more suitable than the GGA–PBEsol (as described in Section 2.2). Hence, in such calculations and some other exceptions, the GGA–PBE has been used instead of the GGA–PBEsol.

2. Methodology

The aforementioned properties are calculated using the VASP 5.2 first principles code. Calculations are performed using the MedeA [20] interface. The elastic property calculations are performed using the MT module of MedeA. Structure building modules are used to create the unique supercells and big unit cells required for the calculations of cleavage and cohesive energies, respectively. The phonon calculations required for computing the heat capacity are done through the Phonon module of MedeA. The computational parameters used are tabulated in Table 1

2.1. Elastic properties

The initial crystal structures of the compounds for the calculations are taken from the ICSD [22] database. After a structure optimization run, the optimized structure is given normal and shear strains and the energies of the respective structures are calculated by VASP. The elastic constants are uniquely determined from the calculated energy values. For example, for a given applied engineering strain (the normal strains e_1, e_2 and e_3 and the shear strains e_4, e_5 and e_6), the energy change due to the deformation with respect to the original undistorted lattice (V_0, E_0 being the respective unit cell volume and energy of the undistorted lattice) is,

$$U = \frac{E_{tot} - E_0}{V_0} = \frac{1}{2}\sum_{i=1}^{6}\sum_{j=1}^{6} C_{ij} e_i e_j$$

Here, E_{tot} is the energy of the strained lattice and C_{ij} are the elastic constants of the system. After the C_{ij} are determined, the elastic, bulk and shear moduli are calculated using the Voigt–Reuβ–Hill method. Once the elastic moduli are calculated, the velocities of the transverse and longitudinal acoustic modes can be calculated and the Debye temperature (Θ_D) at 0 K can hence be calculated (see for example [37]).

2.2. Energy of formation

The structures obtained from the ICSD database are subjected to a structure relaxation run to determine the respective energies of formation values (or enthalpy of formation at 0 K). Both functionals supplied with VASP (the older PBE and the newer PBEsol) have been used to check for differences in values predicted. The energy of formation, for a given compound is determined using the equation,

$$\Delta_f E(\text{Compound}) = E_{VASP}(\text{Compound}) - \sum_{i=elements} E_{VASP_i}$$

The calculations for the carbides were done with respect to the VASP energy calculated for diamond. Since the ground state of carbon at 0 K is graphite, the energy of formation for carbides should be calculated with respect to it. Hence the energy of transformation of diamond to graphite was added to obtain the correct energies of formation. In order to calculate the energy of formation of nitrides, it is necessary to calculate the energy of a nitrogen molecule (or a nitrogen-dimer). However, the PBEsol functional, being optimized for densely packed ionic solids, does not handle the 'isolated' nitrogen molecule well and hence ends up overestimating its energy, which in turn underestimates the energy of formation value for the nitrides by a huge extent (~40 eV). Hence, such calculations using the PBEsol functional have not been carried out for the nitride systems.

Table 1
VASP input parameters.

Version	5.2
Potential	PAW
Exchange–correlation functional	GGA–PBEsol/PBE
Energy cut-off	500 eV
k-Point spacing	≤0.2/Å
Geometric convergence factor	0.002 eV/Å
SCF convergence	10^{-7} eV
Integration scheme	Tetrahedral with Bloechl corrections
Strain increment (MT)	0.005
Atomic displacement (Phonon)	±0.02 Å
Supercell transformation (Phonon)	2 * 2 * 2

2.3. Cohesive energy

Experimentally, cohesive energies are calculated from heats of sublimation (extrapolated to 0 K). One could also calculate cohesive energies if formation enthalpies of the corresponding gas phase is known. Cohesive energy, under first principles calculations, is given by the relation,

$$E_{cohesive}(\text{Solid}) = \sum_{i=elements} E_{VASP_i}(\text{Isolated atom}) - \frac{E_{VASP}(\text{Solid})}{\text{Total number of atoms}}$$

Current calculations of cohesive energy were done through the PBE functional since the PBEsol functional does not treat 'isolated' atoms very well as has been explained in Section 2.2.

2.4. Cleavage energy

Cleavage energy is the energy required 'cleave' a material or split it into two parts. The cleavage can correspond to a bulk material, a grain boundary or an interface. In case of cleavage of a bulk material, if the interfaces arising out of the result are identical, then half the energy required for cleavage is given as the 'surface energy' (γ) of the newly formed interface. Cleavage energy can thus correspond to the effectiveness of bonding that has taken place over a plane, which is proportional to the number of bonds arising out of the surface. The plane with the least energy required to cause a cleavage is likely to be classified as the 'cleavage plane' of the solid.

In order to calculate cleavage energy through first principles, one first needs to create a supercell with respect to the plane of interest (say (1 1 1) or (1 0 0)). The single point energy of this supercell is calculated for reference. Then the supercell is split into either 2 identical slabs (the atom terminating the both the slabs should be identical) or 3 non-identical slabs (different atoms causing termination of the slabs) and the energies of the individual slabs are calculated. In the current scenario, the 3-slab model[20] was used (Fig. 1). The cleavage energy, hence, for the given plane (where A is the surface area in the supercell), is given as,

$$E_{cleavage} = \frac{1}{2A}(E^A_{slab} + E^B_{slab} - E_{bulk})$$

2.5. p vs. V calculations

The bulk modulus can be calculated by doing structure optimization calculations at different pressure (an external hydrostatic pressure can be applied during a structure optimization run in VASP) and finding the 'equilibrium' unit cell volume at those specific pressures. The volumes and the corresponding pressures at which they are stable can then be fitted into a polynomial function (cubic function was found to be the most efficient for the current systems). The derivative of this function will then give rise to the bulk modulus.

$$\beta(V) = -V\frac{\partial p}{\partial V}$$

As a sanity check, MT module calculations were also performed at the different pressures. The resulting bulk modulus were cross-checked with the ones obtained from the cubic fit. Once bulk modulus values are obtained at different pressures, the first derivative of bulk modulus with pressure can also be calculated.

$$\beta' = \frac{\partial \beta}{\partial p}$$

2.6. Phonon calculations

Phonon calculations are done to obtain the values of heat capacity at constant volume (c_v), the Helmholtz energy (A) and so on at various temperatures. A structurally optimized structure is taken initially and a 'supercell' is created out of this. The supercell is then subjected to perturbations and the energies of the perturbed structures are calculated. Using these the phonon dispersion spectrum and the density of states are obtained, from which the c_v data is obtained.

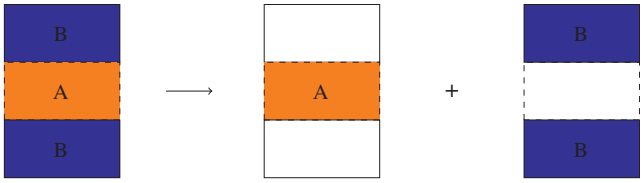

Fig. 1. Illustration of the slab model used for cleavage energy calculations.

Table 2
Experimental and calculated lattice constant values.

Material	Lattice constant (Å)	
	PCD [21]	Calculated
TiC	4.290, 4.642	4.297
TiN	4.221, 4.260	4.210
ZrC	4.470, 4.894	4.685
ZrN	4.561, 4.585	4.576
VC	4.128, 4.180	4.125
VN	4.030, 4.169	4.083
NbC	4.400, 4.670	4.472
NbN	4.368, 4.391	4.412
MoC	4.252, 4.282	4.348
HfC	4.460, 4.674	4.608
TaC	4.433, 4.530	4.446

Table 4
Debye temperature at 0 K.

Material	Debye temperature (K)
TiC	927.1
TiN	945.3
ZrC	689.6
ZrN	661.3
VC	977.5
VN	810.9
NbC	763.9
NbN	595.1
MoC	663.1
HfC	550.3
TaC	588.3

3. Results and discussion

3.1. Lattice constants

Table 2 lists the optimized lattice constant values for all systems under consideration after the structure optimization step. The optimized values are compared with those from Pearson's Crystal Data (PCD) release 2008/9 [21]. For each system Table 2, there are two values reported from PCD. First one corresponds to the lowest and second one the highest reported. It is interesting to note that calculated lattice constants for NbC, NbN and MoC is somewhat higher than experimental values.

3.2. Elastic properties

Table 3 lists the elastic properties calculated for all systems using PBEsol functional. For many of the systems, a good agreement is seen between the calculated values and the reported values (±10%). However, large deviations, especially with values obtained for the Young's modulus are noticed for systems such as NbN, VC and HfC. The calculated values listed below have been subjected through several iterations, including minor changes in the computational parameters used but the results have always been consistent. Hence the deviations might be due to the presence of impurities, vacancies and other such defects (which are not included in the present calculations), slight inaccuracies in experimental measurements and the temperature dependence of the elastic properties. However, it must also be understood that measuring elastic properties of such systems is fraught with difficulties. Also, most of the experimental measurements correspond to polycrystalline samples at ambient temperatures whereas using VASP we obtain the elastic properties of an infinite single crystal at 0 K, a fact which has to be kept in mind. Table 4 lists the calculated Debye temperature (at 0 K) values for all systems. HfC has the lowest Debye temperature while VC has the highest.

3.2.1. CrN: mechanical instability

The stability of a phase at 0 K is entirely dependent on its enthalpy contributions, since the entropy contributions are 0. The equilibrium crystal structure of CrN at 0 K is orthorhombic, which is stabilized by the magnetic stress created by the transformation of Cr to its anti-ferromagnetic state. Also, only the hexagonal structure of MoC is stable at lower temperatures. Such high temperature structures can become 'mechanically unstable' at 0 K if atomic displacements in certain directions cause a decrease in enthalpy compared to the 'optimized structure'. For example, in the case of some high-temperature BCC phases, the strain required $(\varepsilon, -\varepsilon, 0, 0, 0, 0)$ to calculate the tetragonal shear modulus $(\frac{C_{11}-C_{12}}{2})$ causes the structure to become mechanically unstable leading to a 'negative' value for the modulus. Such displacements of atoms and further optimization of the structure may finally lead to the atoms re-positioning themselves away from the high temperature structure (i.e., away from the lattice positions of the cubic phase).

Table 3
Experimental and calculated elastic properties (PBEsol).

Material		C_{11} (GPa)	C_{12} (GPa)	C_{44} (GPa)	E (GPa)	B (GPa)	G (GPa)	v
TiC	Exp.	500 [23]	113 [23]	175 [23]	451 [23]	242 [24]	187 [24]	0.189 [25]
	Calc.	557	124	163	448	268	183	0.22
TiN	Exp.	625 [23]	165 [23]	163 [23]	463 [24]	277 [24]	189 [24]	0.222 [23]
	Calc.	644	129	169	492	300	200	0.227
ZrC	Exp.				403 [23]		165 [26]	0.19 [23]
	Calc.	482	113	146	392	236	160	0.223
ZrN	Exp.				389 [23]		154 [23]	0.259 [23]
	Calc.	572	113	115	384	266	153	0.259
NbC	Exp.				580 [23]		197–245 [26]	0.22 [26]
	Calc.	699	130	170	515	320	209	0.231
NbN	Exp.	556 [23]	152 [23]	125 [23]	480 [23]			
	Calc.	766	116	82	385	148	333	0.299
VC	Exp.				430 [23]		157 [26]	0.22 [26]
	Calc.	705	141	190	546	329	223	0.224
VN	Exp.	533 [23]	135 [23]	133 [23]	460 [23]			
	Calc.	664	186	118	409	345	157	0.302
TaC	Exp.				560 [23]		215–227 [26]	0.24 [26]
	Calc.	778	128	181	563	344	229	0.227
HfC	Exp.				352 [26]			0.18 [26]
	Calc.	551	105	175	461	254	192	0.197
MoC	Exp.							
	Calc.	708	186	119	426	360	164	0.302

Table 5
Calculated and experimental/reported values of the energy of formation.

Material	Energy of formation (kJ mol^{-1})		
	Calculated		Experimental/reported
	PBEsol	PBE	
ZrC	−167	−168	−197 [29]
ZrN		−326	−365 [29]
NbC	−100	−104	−144 [29]
NbN		−169	−227 [38]
VC	−96	−90	−100 [38]
VN		−189	−217 [29]
TaC	−127	−123	−144 [29]
HfC	−196	−193	−209 [41]
MoC	27	31	+23 [30]
TiC	−172	−168	−184 [29]
TiN		−334	−336.7 [31]

Table 6
Calculated and reported values of cohesive energies of pure elements.

Element	Energy (kJ mol^{-1})	
	Cohesive (PBE)	$\Delta_f E$ of gas phase
Ti	519	470 [32]
Zr	606	609 [32]
Nb	708	726 [33]
V	514	514 [33]
Ta	797	782 [33]
Hf	620	619 [33]
Mo	702	658 [33]
C (diamond)	752	751 [20]
N (dimer)	503	477 [34]

Table 7
Calculated values (PBE) of cohesive energies of systems under consideration.

Material	Cohesive energy (kJ mol^{-1})	Melting point (K)
TiC	535	3433
TiN	407	3203
ZrC	590	3805
ZrN	458	3253
NbC	586	3763
NbN	409	2846
VC	434	3083
VN	272	2323
TaC	599	4153
HfC	549	4215
MoC	476	...

Such mechanical instability problems have so far not been addressed by conventional ab-initio calculations. Recent attempts [27,28] have tried to fix the issue by the usage of the SCAILD algorithm and large-displacement phonon calculations, albeit in a round-about fashion. During the calculations of the elastic properties of CrN, its mechanical instability was found out. Since, for calculations of elastic properties, specific displacements of the CrN BCC structure are required, the same calculations have not been carried out due to the uncertainty in the results, created by a mechanically unstable structure. However, the high temperature BCC phase of MoC was not found to be mechanically unstable and as has been listed in Table 3, its elastic properties have been calculated. Also, it must be kept in mind that the BCC MoC phase exists as a sub-stoichiometric (C-deficit) phase, which is not taken into account in the present calculations.

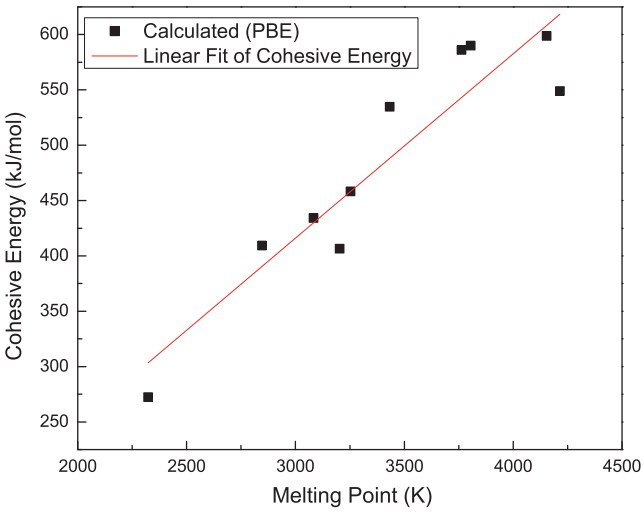

Fig. 2. Cohesive energy vs. melting point.

Table 8
Calculated (PBEsol) cleavage energies of the respective (111) planes.

Material	Energy (J m^{-2})	
	Calculated	Reported
TiN	7.88	6.77 [20]
TiC	11.72	
ZrC	10.15	
ZrN	6.39	
VC	9.55	
VN	5.77	
NbC	8.41	
NbN	5.31	
MoC	6.22	
TaC	11.28	
HfC	9.05	

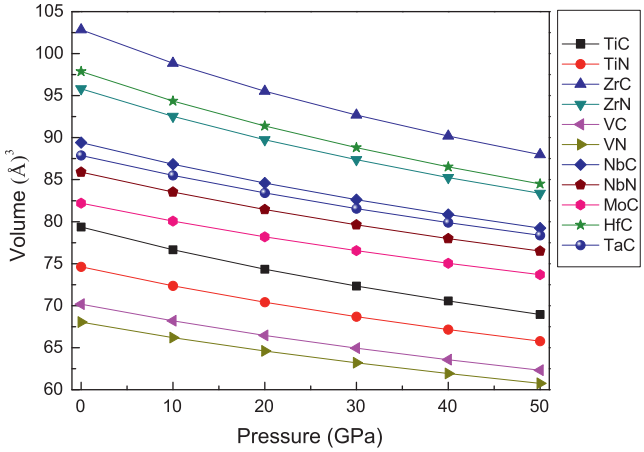

Fig. 3. Pressure vs. unit cell volume.

3.3. Energy of formation

Table 5 lists the calculated energies of formation values (or enthalpy of formation at 0 K). The calculated values differ from the reported values by ≈30 kJ mol^{-1} (which relatively corresponds to an error of 11–40%) for all systems except for TiC and TiN. The

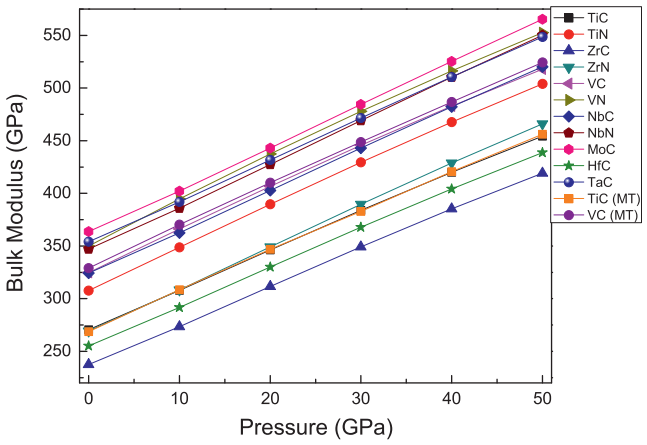

Fig. 4. Pressure vs. bulk modulus obtained from derivative of the p–V relation. MT module results of TiC and VC are also displayed.

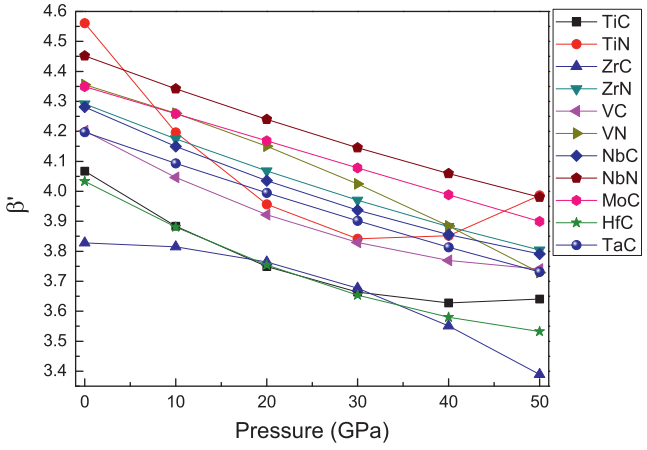

Fig. 5. Pressure vs. β'.

differences can be attributed to both temperature contributions and errors in the experimental measurements. It is also interesting to note the positive energy of formation for MoC, which simply reinforces the thermodynamic instability of cubic MoC at 0 K.

3.4. Cohesive energy

Heat of sublimation or the formation enthalpy of the vapor phase of a given solid indicates the amount of energy required for the transformation of the solid phase into the gas phase. With the atomic interactions being extremely low in the gas phase, this scenario can be approximated to atoms being isolated. Hence, the heat of sublimation or the formation enthalpy of the gas phase can be approximated to the cohesive energy of the solid. However, there are no reported values of the heat of sublimation or formation enthalpy of the vapor phase for the carbides and nitrides under consideration, but such values are available for the pure elements. As can be observed in Table 6, there is a good correspondence between reported and calculated cohesive energy values for the standard reference states for pure elements except for Ti and Mo.

Since the cohesive energy calculations of pure elements were reasonably accurate, it is assumed that the current cohesive energy calculations for the systems under consideration will also be reasonably accurate. Table 7 indicates the calculated cohesive energy values and the corresponding melting points of the particular systems. There seems to be a good correlation in the cohesive energy predicted and the melting points (higher cohesive energies should lead to higher melting points). As for MoC, the sub-stoichiometric cubic phase (0.42 at.% C) melts at ~2800 K and the system under consideration is the stoichiometric cubic phase. Hence, it can only be said with certainty that the cubic phase will melt at a temperature >2800 K, while it cannot be determined experimentally.

Fig. 2 represents a plot of cohesive energies and melting points. A linear fit is also shown in the figure.

3.5. Cleavage energy

Table 8 indicates the calculated cleavage energies. The deviations caused in the case of TiN can be attributed to the difference in the optimized cell-size (and hence different slab thicknesses) between the one reported in [20] and the current calculations. To the best of our knowledge, there were no other reported or experimental values to compare with for the other systems. All the calculated values are for the respective (1 1 1) planes.

3.6. p vs. V calculations

Fig. 3 depicts the results of the calculations done at various external hydrostatic pressures. The corresponding cubic fits made

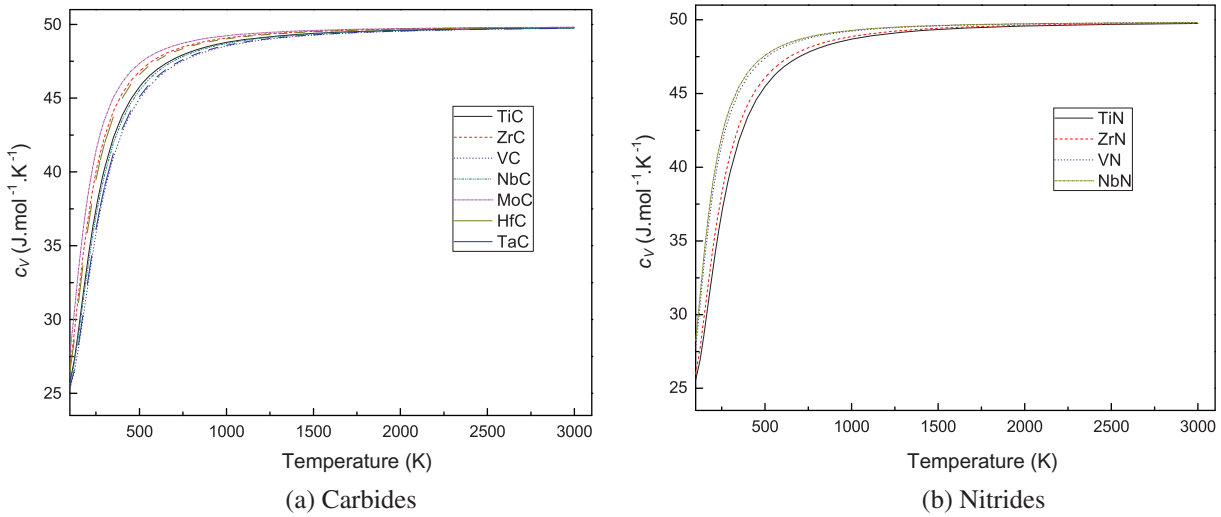

Fig. 6. c_v vs. temperature.

Table 9
Comparison of calculated and reported heat capacity values.

Material	Heat capacity (J mol^{-1} K^{-1})			
	298 K		1000 K	
	Present work	Calphad TCFE7 [38]/SGTE [39]/HSC [32]	Present work	Calphad TCFE7 [38]/SGTE [39]/HSC [32]
TiC	40.18	33.61/33.80/39.38	48.77	51.02/51.20/49.93
TiN	39.61	37.06/37.06/38.40	48.68	52.60/52.17/55.07
ZrC	42.33	38.63 [40]/37.88/40.86	49.08	50.47 [40]/53.39/46.93
ZrN	40.81	40.55/40.45/39.88	48.87	49.21/52.75/52.08
VC	38.66	31.78/. . ./42.05	48.53	51.71/. . ./55.72
VN	43.60	40.70/37.97/41.07	49.24	46.98/53.72/60.87
NbC	39.75	36.96/36.85/40.79	48.71	51.09/51.16/46.00
NbN	44.05	42.99/38.98/39.81	49.29	48.34/53.09/51.14
MoC	43.50	49.30/37.59/42.75	49.22	51.55/56.06/49.98
TaC	38.93	33.21/36.78/42.98	48.58	51.07/51.05/49.70
HfC	41.88	37.56 [41]/34.41/45.58	49.02	50.62 [41]/51.59/52.94

between p and V. As expected, the equilibrium volume decreases with increase in external pressure and the bulk modulus increases with increase in pressure. Calculations at the above mentioned pressures were also done through the MT module (i.e., by applying strains to the structure) and the bulk modulus calculated through the same, as a sanity check.

As can be seen in the case of TiC and VC in Fig. 4, there is a very good match between the bulk modulus obtained from the p vs. V fit and the one obtained through the MT module (±10%). Similar trend was observed for all the other systems.

The first derivative of bulk modulus with respect to pressure was also determined. As indicated by Fig. 5, the positive value of β' indicates that the bulk modulus increases with the increase in pressure. It is quite interesting to note that β' increases with pressure for TiC and TiN systems while this behavior is not replicated in the other systems.

3.7. Phonon calculations

The heat capacity (c_v) values calculated for all the carbides and nitrides are plotted in Fig. 6a and b, respectively. As expected, at high temperatures the c_v values for all systems approach 49 J/mol K ($6R$). The heat capacity values for all systems are also listed at two temperatures (298 K and 1000 K) in Table 9. These are compared with heat capacity (c_p) values obtained from thermodynamic functions [32,38–40], although c_v values must be somewhat lower c_p values especially at higher temperatures. It should also be mentioned that electronic contribution to heat capacity not included in the present calculations.

4. Conclusions

The elastic properties such as the elastic constants, the Young's modulus, the bulk modulus, the shear modulus, Poisson's ratio and the cleavage energies of the (1 1 1) planes, thermochemical properties such as the energy of formation, cohesive energy and physical properties like the pressure–volume relationship, the first derivative of bulk modulus, the Debye temperature and the heat capacity at constant volume are successfully calculated for the rock salt-type transition metal carbide and nitride systems under consideration. All values reported here are entirely obtained through first principle calculations. Wherever possible, calculated values are compared with experimental (or other calculated) values. In most case good match is seen.

References

[1] E.K. Storms, The Refractory Carbides, Academic Press, New York/London, 1967.
[2] L. Toth, Transition Metal Carbides and Nitrides, Academic Press, New York, 1971.
[3] The Physics and Chemistry of Carbides, Nitrides and Borides, in: S.T. Oyama (Ed.), Blacklie Academic and Professional, London, 1996.
[4] NIST, National Institute of Standards and Technology, 1988 <http://www.nist.gov/>.
[5] F. Peng, L. Han, H. Fu, X. Cheng, First-principles calculations on elasticity and the thermodynamic properties of TaC under pressure, Phys. Status Solidi B 246 (2009) 1590–1596.
[6] V. Krasnenko, M. Brik, First principles calculations of hydrostatic pressure effects on structural, elastic and thermodynamic properties of cubic monocarbides XC (X = Ti, V, Cr, Nb, Mo, Hf), Solid State Sci. 14 (2012) 1431–1444.
[7] Y. Yang, H. Lu, C. Yu, J. Chen, First principle calculations of mechanical properties of TiC and TiN, J. Alloys Compd. 485 (2009) 542–547.
[8] D.H. Fors, G. Wahnström, First-principles investigations of the stability of MN and CrMN precipitates under coherency strains in α-Fe (M = V, Nb, Ta), J. Appl. Phys. 109 (2011) 113709.
[9] P. Lazar, R. Podloucky, E. Kozeschnik, J. Redinger, Density functional theory study of ternary V–Cr–N compounds, Phys. Rev. B: Condens. Matter Mater. Phys 78 (2008) 134202.
[10] W. Feng, S. Cui, H. Hu, G. Zhang, Z. Lv, Electronic structure and elastic constants of TiC_xN_{1-x}, $Zr_xNb_{1-x}C$ and HfC_xN_{1-x} alloys: a first-principles study, Physica B 406 (19) (2011) 3631–3635.
[11] R. Yu, Y. Jiang, J. Feng, R. Zhou, Y. Zhang, R. Zhou, The stability and elastic properties of NaCl-type MN (M = Ti, V, Zr, Nb, and Ta) compounds investigated by first principles, J. Mater. Sci. 48 (9) (2013) 3443–3447.
[12] J. Kim, S. Kang, Elastic and thermo-physical properties of TiC, TiN, and their intermediate composition alloys using ab initio calculations, J. Alloys Compd. 528 (2012) 20–27.
[13] K. Jiwoong, S. Kang, First principles investigation of temperature and pressure dependent elastic properties of ZrC and ZrN using Debye–Grüneisen theory, J. Alloys Compd. 540 (0) (2012) 94–99.
[14] J. Zhu, B. Zhu, J.Y. Qu, Q.Q. Gou, F. Chen, Thermodynamic properties of cubic ZrC under high pressure from first-principles calculations, Sci. China Ser. G: Phys. Mech. Astronomy 52 (2009) 1039–1042.
[15] VASP, Software, 1995 <http://www.vasp.at/>.
[16] M. Segall, P. Lindan, M. Probert, C. Pickard, P. Hasnip, S. Clark, M. Payne, First-principles simulation: ideas, illustrations and the CASTEP code, J. Phys.: Condens. Matter 14 (2002) 2717.
[17] Materials-Studio, Software Package <http://accelrys.com/products/materials-studio/>.
[18] G. Kresse, J. Joubert, From ultrasoft pseudopotentials to the projector augmented wave method, Phys. Rev. B: Condens. Matter Mater. Phys. 59 (1999) 1758.
[19] J.P. Perdew, A. Ruzsinsky, G.I. Csonka, O.A. Constantin, X. Zhou, K. Burke, Restoring the density–gradient expansion for exchange in solids and surfaces, Phys. Rev. Lett. 100 (2008) 136406.
[20] MedeA, Software package <http://www.materialsdesign.com/medea>.
[21] P. Villars, K. Cenzual, Pearson's Crystal Data: Crystal Structure Database for Inorganic Compounds, Release 2008/9, ASM International, Materials Pasrk, Ohio, USA.
[22] ICSD, Database <http://www.fiz-karlsruhe.de/icsd.html>.
[23] NIST-Ceramics, Database <http://www.ceramics.nist.gov>.
[24] Q. Yang, W. Lengauer, T. Koch, M. Scheerer, I. Smid, Hardness and elastic properties of $Ti(C_xN_{(1-x)})$, $Zr(C_xN_{(1-x)})$ and $Hf(C_xN_{(1-x)})$, J. Alloys Compd. 309 (2009) L5–L9.
[25] J.F. Shackelford, W. Alexander (Eds.), CRC Materials Science and Engineering Handbook, third ed., CRC Press LLC, Boca Raton, Florida 33431, USA, 2001.
[26] MatWeb, Database <http://www.matweb.com>.
[27] P. Souvatzisa, O. Erikssona, M. Katsnelsonb, S. Rudinc, The self-consistent ab initio lattice dynamical method, Comput. Mater. Sci. 44 (2009) 888–894.
[28] N. Antolin, O.D. Restrepo, W. Windl, Fast free energy calculations for unstable high-temperature phases, Phys. Rev. B: Condens. Matter Mater. Phys 86 (2012) 054119.
[29] Malcolm W. Chase Jr., NIST–JANAF thermochemical tables, J. Phys. Chem. Ref. Data Monograph 9 (1998) 1–1951. Fourth edition.

[30] W. Mihalkovic, Alloy database, 2009 <http://alloy.phys.cmu.edu>.
[31] S.G. Fries, T. Jantzen, Compilation of CALPHAD formation enthalpy data: binary intermetallic compounds in the COST 507 Gibbsian database, Thermochim. Acta 314 (1998) 23–33.
[32] A. Roine, Outokumpu HSC chemistry for windows v7.193: chemical reaction and equilibrium software with extensive thermochemical database Pori, Finland: Outokumpu, 1999 <http://www.outotec.com/en/Products-services/HSC-Chemistry/>.
[33] Chemistry-Reference, Database. URL http://www.chemistry-reference.com/.
[34] J. Harl, G. Kresse, Cohesive energy curves for noble gas solids calculated by adiabatic connection fluctuation–dissipation theory, Phys. Rev. B: Condens. Matter Mater. Phys. 77 (2008) 045136.
[35] Burke Research Group, Website <http://dft.uci.edu/research.php#pbe>.
[36] M. De La Pierre, R. Orlando, L. Maschio, K. Doll, P. Ugliengo, R. Dovesi, Performance of six functionals (LDA, PBE, PBESOL, B3LYP, PBE0, and WC1LYP) in the simulation of vibrational and dielectric properties of crystalline Compounds. The case of forsterite Mg_2SiO_4, J. Comput. Chem. 32 (2011) 1775–1784.
[37] J. De Klerk, Elastic constants and Debye temperature of TiC using a new ultrasonic coherent pulse/cw technique, Rev. Sci. Instrum. 36 (1965) 1540–1545.
[38] TCS steels/Fe-alloys database v7.0, Thermo-Calc Software AB, Sweden <http://www.thermocalc.se/>.
[39] SGTE Substances Database, Scientific Group Thermodata Europe, 2012.
[40] A.F. Guillermet, Analysis of thermochemical properties and phase stability in the zirconium–carbon system, J. Alloys Compd. 217 (1995) 69–89.
[41] H. Bitterman, P. Rogl, Critical assessment and thermodynamic calculation of the binary system Hafnium–Carbon (Hf–C), J. Phase Equilibr. 18 (1997) 344–356.